HAL
open science

Revisiting low temperature oxidation chemistry of n-heptane

Cheng Xie, Maxence Lailliau, Gani Issayev, Qiang Xu, Weiye Chen, Philippe Dagaut, Aamir Farooq, S. Mani Sarathy, Lixia Wei, Zhandong Wang

To cite this version:

Cheng Xie, Maxence Lailliau, Gani Issayev, Qiang Xu, Weiye Chen, et al.. Revisiting low temperature oxidation chemistry of n-heptane. Combustion and Flame, 2022, 242, pp.112177. 10.1016/j.combustflame.2022.112177 . hal-03684380

HAL Id: hal-03684380

https://hal.science/hal-03684380v1

Submitted on 1 Jun 2022

HAL is a multi-disciplinary open access archive for the deposit and dissemination of scientific research documents, whether they are published or not. The documents may come from teaching and research institutions in France or abroad, or from public or private research centers.

L'archive ouverte pluridisciplinaire **HAL**, est destinée au dépôt et à la diffusion de documents scientifiques de niveau recherche, publiés ou non, émanant des établissements d'enseignement et de recherche français ou étrangers, des laboratoires publics ou privés.

Copyright

Revisiting low temperature oxidation chemistry of *n*-heptane

Cheng Xie [a], Maxence Lailliau [b], Gani Issayev [c], Qiang Xu [a], Weiye Chen [a], Philippe Dagaut [b], Aamir Farooq [c], S. Mani Sarathy [c], Lixia Wei [d], Zhandong Wang [a,e,f] *

[a] *National Synchrotron Radiation Laboratory, University of Science and Technology of China, Hefei, Anhui 230029, PR China*

[b] *Centre National de la Recherche Scientifique (CNRS), INSIS, ICARE, 1C Avenue de la Recherche Scientifique, 45071, Orléans, cedex 2, France*

[c] *King Abdullah University of Science and Technology (KAUST), Clean Combustion Research Center (CCRC), Physical Sciences and Engineering Division, Thuwal 23955-6900, Saudi Arabia*

[d] *College of Mechanical Engineering, Guangxi University, Nanning, Guangxi 530004, PR China*

[e] *State Key Laboratory of Fire Science, University of Science and Technology of China, Hefei, Anhui 230026, PR China*

[f] *Dalian National Laboratory for Clean Energy, Dalian 116023, China*

Abstract: Benefitting from the rapid development of instrumental analysis methods, intermediate products that were difficult to probe in the past can now be measured and quantified in complex reaction systems. To understand low temperature reactions of interest for combustion applications, and reduce the deviations between model predictions and experimental measurements, constant advancement in understanding low temperature oxidation process is necessary. This work examines the oxidation of *n*-heptane in jet-stirred reactors at atmospheric pressure, with an initial *n*-heptane mole fraction of 0.005, equivalence ratio of 0.5, a residence time of 1s, and over a temperature range of 500-800 K. Reaction products were analyzed using synchrotron ultra-violet photoionization mass spectrometry, gas chromatography, and Fourier-transform infrared spectroscopy. Ignition delay times of *n*-heptane/O_2/CO_2 mixture were measured in a rapid compression machine at 20 and 40 bar over a 600-673 K temperature range. Based on the experimental results, a comprehensive kinetic model of *n*-heptane low temperature oxidation was developed by considering the sub-mechanisms of keto-hydroperoxide, cyclic ether, heptene isomers, and the third O_2 addition reaction, and by

* Corresponding author: E-mail: zhdwang@ustc.edu.cn (Z. Wang)

updating the rate constants of keto-hydroperoxide decomposition and second oxygen addition reactions. The combination of reaction mechanism development and evaluation of the rate constants of key reactions enabled the model to effectively predict the species concentrations and ignition delay times of *n*-heptane low temperature oxidation, providing additional insight into alkane low temperature oxidation chemistry.

Keywords: kinetic modeling; low temperature oxidation; Korcek reaction; ignition delay time; third oxygen addition

1. Introduction

Global warming is of worldwide concern, and excessive carbon emissions are believed to be its main cause. According to statistical data from the European Union, automobile exhaust emissions account for approximately 12% of the total emissions of carbon dioxide [1]. Because of its high efficiency and low emission operation [2], advanced compression-ignition (ACI) has become a reliable technology for future reduction of carbon emissions from internal combustion engines, and, since ACI technology relies strongly on low temperature ignition chemistry, it is important to improve our understanding of low temperature combustion behavior of liquid fuels [3].

The low temperature oxidation mechanism of *n*-heptane has been studied extensively, since it is a primary reference fuel [4-7] often used as a component of surrogate fuels representing gasoline and diesel. As early as the 1970s, Coats and Williams developed a kinetic model of *n*-heptane oxidation containing 27 species, to simulate ignition and combustion of *n*-heptane/oxygen/argon mixtures [8]. In 1989, Westbrook *et al.* [9] developed a detailed kinetic model of *n*-heptane and *iso*-octane which included 765 reversible reactions and 212 species. Their kinetic model was compared with the experimental results measured from the shock tube, turbulent flow reactor and low temperature static and stirred reactors. Curran *et al*. [10] developed a comprehensive kinetic model of *n*-heptane oxidation by proposing the low and high temperature oxidation reaction classes. This

model--including 2450 elementary reactions and 550 species--was validated by global combustion properties and speciation data of *n*-heptane oxidation in the literature. Ranzi *et al.* [11] proposed a semi-detailed kinetic scheme for *n*-heptane oxidation by comparing modeling predictions with experimental data over a wide range of temperature (550-1600K), pressure (6-40 bar) and equivalence ratio (0.3-2). Herbinet *et al*. studied the *n*-heptane low and high temperature oxidation in a jet-stirred reactor (JSR) by gas chromatography (GC) and synchrotron vacuum ultraviolet photoionization mass spectrometry (SVUV-PIMS) over temperatures ranging from 500 to 1100 K, with a residence time of 2 s and atmospheric pressure [12]. Keto-hydroperoxides (KHP), heptadiones, and carboxylic acids like acetic acid and propionic acid were measured. A kinetic model was generated with the EXGAS software, and reactions forming diones, acetic acid, propanoic acid, methyl vinyl ketone, 2-butenal, 1,3-pentadiene, 1,4-heptadiene, and 2-hexanone were added to predict their experimental measurements. Rodriguez *et al.* detected many hydroperoxide intermediates, ketene and diones during the *n*-heptane and *n*-decane gas-phase oxidation; they also calculated the ionization energy of the most probable isomers derived from *n*-heptane oxidation [13]. Ranzi *et al.* extended the reaction classes for the low temperature oxidation, e.g., H-abstraction reactions on hydroperoxides which forms ketones, H-abstraction reactions on keto-hydroperoxides that forms diones, the Korcek reaction of KHP, and the recombination/disproportionation reactions of peroxy and hydroperoxy-alkylperoxy radicals that form alcohols and different oxygenated species [14]. Zhang *et al*. [15] updated the kinetic model of *n*-heptane oxidation by using the newly proposed rate rules for alkanes such as pentane isomers and *n*-hexane. The kinetic model satisfactorily predicted the ignition delay time, laminar flame speed, and the chemical species speciation data of *n*-heptane/O_2/dilution gas mixtures.

Recent work by Wang *et al.* [16] probed highly oxygenated intermediates with one to two hydroperoxy groups during the autoxidation of 15 organic compounds at combustion-relevant

temperatures. The peroxy radical reaction mechanism with three stages of sequential O_2 addition was proposed. Subsequently, a detailed species pool analysis of *n*-heptane low temperature oxidation during the JSR and a cooperative fuel research (CRF) engine was carried out by Wang *et al.* [7]; intermediates with the same carbon skeleton as the fuel, such as $C_7H_{10}O_x$ (x=0-4), $C_7H_{12}O_x$ (x=0-4), and $C_7H_{14}O_x$ (x=0-5) were observed. However, the mole fraction profiles of those intermediates were not reported, due to the lack of photoionization cross sections (PICS) for quantification. The bimolecular reactions of the C7 intermediates, (e.g. $C_7H_{14}O_x$ (x = 0–5) and $C_7H_{12}O_x$ (x = 0–4)), and the formation of C2-C6 diones from the decomposition of the C7 keto-alkoxy radicals were discussed to explain the experimental observation. However, these pathways, and the third O_2 addition pathways, were seldom considered in the kinetic models [10, 12, 15, 17, 18].

More recently, Belhadj *et al.* [19] studied the oxidation of 1000 ppm of *n*-heptane in a JSR at 10 atm, and an equivalence ratio of 0.5, at a residence time of 1 s, in a temperature range of 580-790 K. They also oxidized 5000 ppm of fuel at 647 K and a residence time of 1.5s. Several low temperature oxidation products were characterized using an Orbitrap® mass spectrometer (MS) with atmospheric pressure chemical ionizations, flow injection analyses and ultra-high pressure liquid chromatography MS coupling. Among these the formation of hydroperoxides ($C_7H_{16}O_2$), keto-hydroperoxides ($C_7H_{14}O_3$), cyclic ethers ($C_7H_{14}O$), carboxylic acids ($C_2H_4O_2$, $C_3H_6O_2$, $C_4H_8O_2$), ketones ($C_{3\text{-}5}H_{6\text{-}10}O$), diones ($C_7H_{12}O_2$), and highly oxygenated molecules ($C_7H_{14}O_{5,7,9,11}$), resulting from the addition of up to six O_2 molecules on fuel radicals was reported. Several kinetic models were tested against their data, showing significant discrepancies and inaccurate prediction of keto-hydroperoxides formation profile versus temperature.

In this study, *n*-heptane low temperature oxidation was further investigated in a JSR by the combination of SVUV-PIMS, gas chromatography (GC) and Fourier-transform infrared spectroscopy (FTIR) analysis. The first goal was to measure and quantify intermediates that included

C_7H_{14} (heptenes), $C_7H_{14}O$ (cyclic ethers), $C_7H_{14}O_3$ (keto-hydroperoxides and hydroperoxy cyclic ethers), $C_7H_{12}O$ (e.g., heptenones and olefinic cyclic ethers), $C_7H_{12}O_2$ (e.g., diones and keto cyclic ethers), $C_3H_4O_2$ (diones), $C_4H_6O_2$ (diones), $C_5H_6O_2$ (diones), $C_6H_8O_2$ (diones), CH_2O_2 (formic acid), $C_2H_4O_2$ (acetic acid), $C_3H_6O_2$ (propionic acid), and $C_4H_8O_2$ (butyric acid). Species in parentheses are the most probable intermediates with the given brute formula. These intermediates were instructive for examining the first and second O_2 addition reactions of *n*-heptane oxidation, and the reaction mechanism of keto-hydroperoxides and cyclic ethers. Based on the experimental measurement, the second goal of this work was to develop a comprehensive kinetic model of *n*-heptane low temperature oxidation by evaluating the second and third O_2 addition reactions, the reaction mechanism of keto-hydroperoxides, and the reaction mechanism of cyclic ethers. In addition to JSR data, the ignition delay times (IDT) of *n*-heptane low temperature oxidation were measured in a rapid compression machine (RCM) in temperatures ranging from 600-673 K. According to our knowledge, there was no IDT data for *n*-heptane at temperature as low as 600 K and pressure of 20 and 40 bar. The kinetic model was further analyzed and tested using the IDT data measured in this work, and those reported in the literature. In comparison with the model of Zhang *et al*. [15] from the literature, this work adopted different rate rules for the second O_2 addition and the decomposition of the peroxides. Furthermore, it also considered third O_2 addition reactions. The methodology adopted here provides improved understanding of low temperature oxidation model development, to better predict *n*-heptane low temperature behavior measured in JSR and RCM oxidation.

2. Experimental methods

2.1. JSR experiment at NSRL

The JSR SVUV-PIMS experiment in this work was performed at the atomic and molecular physics beamline (BL09U), National Synchrotron Radiation Laboratory (NSRL), University of Science and Technology of China (USTC) in Hefei, China. The atomic and molecular physics

beamline is an undulator-based beamline, designed to operate in the photon energy range of 7.5-124 eV [20]. A detailed description of the experimental setup has been described in previous work [21]; briefly, it is composed of a controlled evaporation and mixing (CEM) system, a jet-stirred reactor, and a molecular beam sampling time-of-flight mass spectrometer, coupled with synchrotron vacuum ultraviolet photoionization.

During the experiment, the CEM system controlled the flow rate of *n*-heptane, and Ar, and the homogenous vaporization of *n*-heptane was achieved. The gas mixture was mixed with O_2 and introduced into the JSR with a volume of 76 cm^3 by way of a heated transfer line. The temperature of the heated transfer line was set as 373 K, and the flow rate of O_2 was controlled by a MKS mass flow controller. In the experiment, the mole fraction of *n*-heptane was 0.005, equivalence ratio was 0.5, the residence time was 1 sec, and the pressure of the experiment was 1 bar. During the JSR oxidation, the composition was sampled by a quartz nozzle with a diameter of 75 μm, then ionized by the SVUV and analyzed with the time-of-flight mass spectrometer. The mass resolution of the time-of-flight mass spectrometer was ca. 5000 at *m/z* 100. C/H/O composition of the low temperature oxidation products could be separated. The uncertainty of the measured reaction temperature was within ± 10 K. The uncertainty of the mole fraction calculated with direct calibration was ± 10%, the uncertainty of the mole fraction calculated with known photoionization cross section (PICS) was estimated to be ± 20%, and the uncertainty of the mole fraction calculated from estimated PICS was a factor of 2 [21]. The *n*-heptane was provided by Aladdin (>99.5%(GC)). Argon and oxygen were provided by Air Liquide with purities of 99.99% and 99.999%, respectively.

2.2. JSR experiment at Orléans

Another JSR experiment was performed at Orléans, France; a detailed description of the experimental setup is available in previous literature [22-25]. The volume of the JSR was 35 cm^3, and the experimental condition for the Orléans experiment was the same as the SVUV-PIMS

experiment, except that the dilution gas was N_2. In the experiment, high purity gases from Air Liquide were used: oxygen >99.995% pure, nitrogen: >99.9 pure (<50 ppm of O_2 and H_2O; <1000 ppm of Ar; <5 ppm of H_2). N-heptane >99.5% pure was from Aldrich. The gas-phase mixture in the reactor was sampled in a low pressure sonic probe and transferred through a Teflon line to the analyzer; of these, the FTIR was used to quantify H_2O, CO, CO_2 and CH_2O. Two gas chromatographs with flame ionization detectors were used to detect the reaction products. One of the GCs was equipped with a DB624 column for detection of oxygenated compounds, the other had a CP-Al_2O_3/KCl column to measure hydrocarbons. The identification of the products was performed by the GC/MS (Shimadzu GC2010 Plus), with 70 eV electron impact as the ionization mode. Uncertainty of temperature measurements was estimated to be less than 10 K, and the uncertainties in the mole fraction were less than 5% for the reactants, and less than 10% for species with mole fractions higher than 10 ppm [26]. In the case of formic acid and acetic acid, error bars could be as high as +/- 10 ppm.

2.3 RCM experiment at KAUST

Ignition delay time (IDT) experiments reported in this work were conducted at the KAUST rapid compression machine (RCM) facility, described in detail in previous publications [27]. The RCM is equipped with a twin-opposed piston design which can attain a volumetric compression ratio of up to 16.8. The reaction chamber is 50.8 mm in diameter, with a stroke length of 169 mm per piston; the pistons were pneumatically driven and arrested at the end of compression (EOC) by a hydraulic locking mechanism. They were designed with creviced heads to suppress roll-up vortex and boundary layer mixing with the core gas, thus enabling the use of adiabatic core hypothesis. A typical experiment took ~ 3 ms for the final 50% pressure rise during piston compression. At EOC, the pressure reached a local maximum which is marked as *time zero*. Ignition delay time is defined as the time period between the EOC and the instant of maximum pressure rise as a result of heat

release from fuel ignition. Pressure profiles were recorded by a Kistler 6045A pressure transducer mounted (PTM) through a port in the combustion chamber. Uncertainty in IDTs measured in the RCM was estimated to be ±10%.

Reactive mixtures (*n*-heptane/O_2/CO_2) were prepared in a 20 L stainless steel mixing vessel equipped with a magnetically driven stirrer, which ensured homogeneity of the mixture in a short time (~ 1 – 2 hours). Another identical vessel was used to prepare non-reactive mixtures (oxygen replaced with CO_2). N-heptane was purchased from Sigma Aldrich with a purity of 99.9%. All other gases (N_2, O_2, Ar) were purchased from AH Gases with purities of 99.999%. Pressure traces measured in non-reactive RCM experiments were used to compute volume time histories to account for heat loss in chemical kinetic simulations. Before mixture preparation, the vessels were turbo-pumped down to 10^{-5} Torr. The experimental conditions of *n*-heptane oxidation in JSRs and RCM are given in Table 1.

Table 1. The experimental conditions of *n*-heptane oxidation

Reactors	Instrument	Place	T	φ	p
JSR-1	SVUV-PIMS	Hefei	500-800	0.5	1 bar
JSR-2	GC	Orléans			
RCM	Kistler PTM	Thuwal	600-673	0.4 and 1	20 and 40 bars

3. Results and discussion

In this study, around 50 oxidation species, such as alkenes, aldehydes, ketones, carboxylic acids, cyclic ethers, diones, peroxides were probed using SVUV-PIMS, FTIR and GC-MS. Furthermore, the low temperature IDTs were measured for the oxidation of *n*-heptane/O_2/CO_2 in the KAUST RCM. A detailed *n*-heptane oxidation mechanism consists of 1818 species and 7452 reactions was developed, based on the *n*-heptane kinetic model from Zhang *et al.* [15], which has 1268 species and

5336 reactions. The thermodynamic data of the species involved have been calculated using the THERM software [28]. Details of the model development is discussed in the following sections.

A schematic representation of the reaction mechanism of alkane low temperature oxidation is presented in Scheme 1. The reaction scheme is based on the current understanding of the reaction mechanism [7, 10, 15, 19, 29-36]. In the reaction process, the fuel consumption is dominated by the H-abstraction from alkane with hydroxyl radicals (OH•) to produce alkyl radicals (R•) [15, 37]. The oxygen addition [15, 34, 37] and intramolecular isomerization reactions [38] that follows formed hydroperoxyalkyl radical (•QOOH). The cyclization of •QOOH radicals release one OH radical and led to the formation of cyclic ethers [32]; this is one of the chain propagation reaction for low temperature oxidation. Further, the second O_2 addition to •QOOH radicals form peroxy alkylhydroperoxide radicals (•OOQOOH) [10, 12, 15, 37, 39]. On one hand, the intramolecular H-migration in •OOQOOH led to keto-hydroperoxides and one OH radical. The weak O-OH bond in the KHP is easily broken and it release another OH radical, creating the main chain branching pathway for low temperature alkane oxidation. However, the intramolecular H-migration in •OOQOOH form other radical intermediates, •P(OOH)$_2$ radicals, which undergo cyclization to form hydroperoxy cyclic ethers (HPCE) and one OH radical. Further decomposition of HPCE led to another OH radical, also creating a chain branching pathway. The addition of O_2 to •P(OOH)$_2$ radicals form •OOP(OOH)$_2$ radicals and initiate the third O_2 addition reaction network.

In Scheme 1, highlighted in blue are reactions discussed here, including second and third O_2 addition reactions, keto-hydroperoxide, cyclic ether, and heptene reactions. The following sections examine the rate rule of the second O_2 addition and C7 KHP decomposition, the reaction sub-mechanisms of C7 KHP, C7 cyclic ether, and heptene, the reaction sub-mechanism of C3-C6 diones, and the third O_2 addition reaction network. The *n*-heptane kinetic model from Zhang *et al.* [15] (named *the NUI model* hereafter) was adopted as the base model for discussion. The reaction sub-

mechanisms of C7 KHP, C7 cyclic ether, and heptene, the reaction sub-mechanism of C3-C6 diones, and the third O_2 addition reaction network were incomplete in the NUI model. A deviation was observed between model predictions and the experimental measurements for the *n*-heptane low temperature oxidation reactivity, the formation of $C_7H_{14}O_3$, $C_7H_{12}O_2$, $C_7H_{12}O$, C1-C4 carboxylic acids, and C3-C6 diones. A more comprehensive reaction mechanism for *n*-heptane low temperature oxidation was then developed. The updated model predicted the speciation data of *n*-heptane low temperature oxidation in the JSR, the IDT data of *n*-heptane low temperature oxidation in the RCM, and the shock tube.

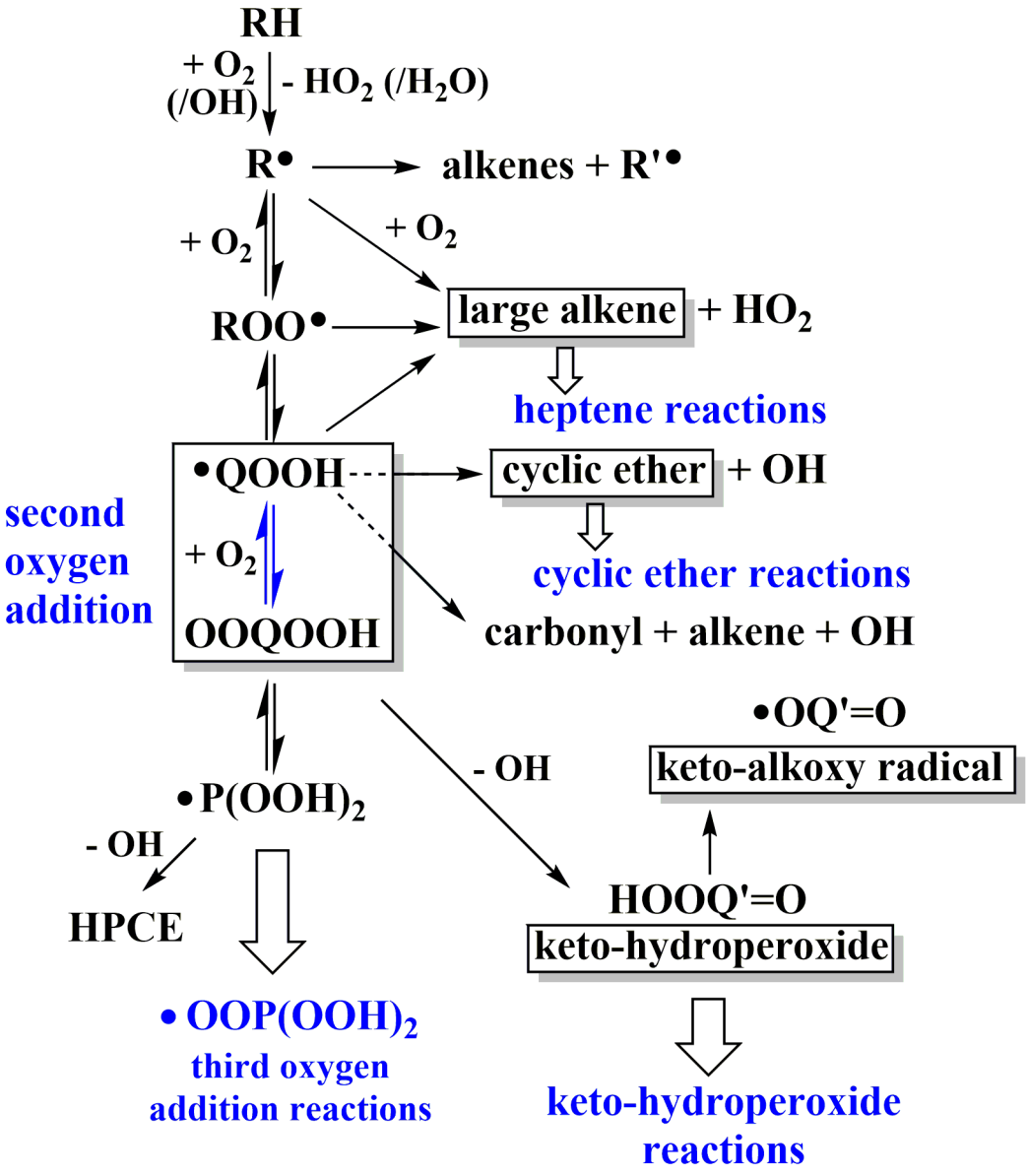

Scheme 1: Schematic of the reaction mechanism of low temperature oxidation of alkanes. Highlighted in blue are reactions discussed here, including second and third O_2 addition reactions, keto-hydroperoxide, cyclic ether, and heptene reactions. The reaction scheme is based on the current understanding of the reaction mechanism [7, 10, 15, 19, 29-36].

3.1 Evaluating the rate constant of second O_2 addition

Reactivity under low temperature oxidation is controlled mainly by a series of oxygen addition and radical isomerization reactions, which determine the carbon flux toward radical chain branching and the concentration of OH radicals. The prediction of oxygen consumption is an important indicator of the accuracy of the kinetic models in order to predict the fuel oxidation process. In the NUI model, the rate constant of the first O_2 addition to alkyl radicals was adopted from theoretical calculations by Miyoshi [34], using a variational transition state theory (VTST) and RRKM/ME methods. The rate constant of the second O_2 addition was derived from the first O_2 addition, with the A-factor decreased by a factor of two [37]. However, the rate constant of the O_2 addition to the 3-hydroperoxyl-1-propyl radical was a factor of two higher than the rate constant of O_2 addition to the *n*-propyl radical by Goldsmith *et al*. [35, 39]. Thus, the assumption that the rate constant of the second O_2 addition was half of the rate constant of first O_2 addition may not be generally valid.

Figure 1 shows experimental data and simulation results for O_2 mole fractions, measured during *n*-heptane low temperature oxidation with an equivalence ratio of 0.5. It can be seen that the prediction of oxygen consumption (> 600 K) was slower than the experimental measurement by the NUI model. In this work, the second O_2 addition rate constant was increased by a factor of two (named *the NUI model-1* hereafter), i.e., the rate constant of the second O_2 addition was the same as the first O_2 addition. The same treatment was applied to the rate constant of the second O_2 addition in the Polimi model [40]. As can be seen in Fig. 1, the consumption of O_2 was promoted, evidently because the carbon flux to the chain-branching pathway was increased and more OH radicals were produced. The dominant source of OH radicals was from the decomposition of KHP; the rate

constant of KHP decomposition had a significant effect on the low temperature oxidation rate. The next section focuses on the KHP decomposition mechanism.

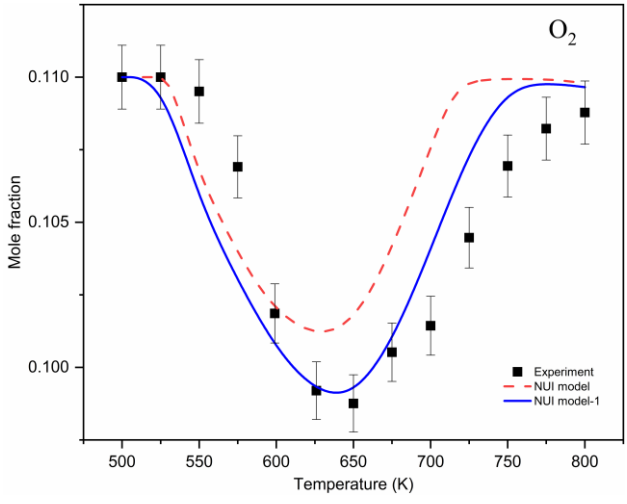

Fig. 1: SVUV-PIMS experiment (symbols) in JSR-1 and modeling results (lines) for oxygen consumption during *n*-heptane JSR oxidation at ϕ = 0.5 and residence time = 1s. Dashed line represents simulation by NUI model, solid line by NUI model-1. Description of models is in the text. The uncertainty of O_2 mole fraction is ± 10%.

3.2 Evaluating the rate constant of C7 KHP decomposition

As shown in Scheme 1, keto-alkoxy radical and an OH radical were formed through the isomerization and decomposition reaction of an •OOQOOH radical. Subsequently, the decomposition of KHP produced another OH radical. These OH radicals produced during the chain branching reactions controlled the low temperature reactivity, therefore, it is important to understand the KHP decomposition mechanism. In the last century, KHP were collected and analyzed by Sahetchian *et al*. [41] in the flow reactor oxidation and CFR engine oxidation of hydrocarbons [42]. In 2010, with the development of combustion diagnostics, Battin-Leclerc *et al*. [43] detected KHP directly in the process of low temperature oxidation of *n*-butane in a JSR, via a molecular beam sampling and SVUV-PIMS analysis.

Although the detection of KHP from low temperature oxidation of hydrocarbons has been extensively reported [7, 16, 19, 31, 41, 43-46], experimental study of the reaction rate constants of

KHP decomposition is scarce. The KHP decomposition rate constant applied in the *n*-heptane oxidation mechanism by Curran *et al.* [10] was estimated by referencing the rate constants of 1-heptyl and 2-heptyl hydroperoxide decomposition, measured by Sahetchian *et al*. in 1991. This rate constant had been widely adopted in low temperature oxidation kinetic models, with the tuning of the decomposition activation energy to better predict the experimental observations. Figure 2a shows the mole fraction of C7 KHP measured in this work and model prediction using the NUI model [15], LLNL [17], Polimi [40] and Bielefeld models [47]. The experimental mole fraction of KHP was the sum of the signal of KHP and its fragment using a total PICS of 6.3 Mb at 10.5 eV, as calculated in the work of Wang *et al*. [44]. It was noted that the mole fraction profile should include the contribution of C7 HPCE, but the dominant component was KHP. The experiment showed that the concentration of the C7 KHP reached its highest value at ca. 580 K, but the NUI, LLNL and Bielefeld models predicted that the C7 KHP mole fraction was toward the lower temperature. In contrast, the Polimi model predicted the temperature dependence of the C7 KHP mole fraction profile well. Figure 2b presents the KHP decomposition rate constants used in these models; it can be seen that the rate constants in the KAUST and Bielefeld models were close, and they were also the fastest. The one used in the NUI model is in the middle, while the one used in the Polimi model is the slowest. The rate constant trend was correlated with the formation of C7 KHP, i.e., the slower rate constant made the decomposition reaction happens at higher temperature. In this work, the C7 KHP decomposition rate constant followed the suggestion of Ranzi *et al*. [14, 40] (i.e., the Polimi model), which predicted the mole fraction profile of KHP versus temperature better. The decomposition of the C7 KHP formed the C7 keto-alkoxyl radicals, which led to the formation of C3-C6 diones by way of the subsequent decomposition. These reactions were also considered in this work.

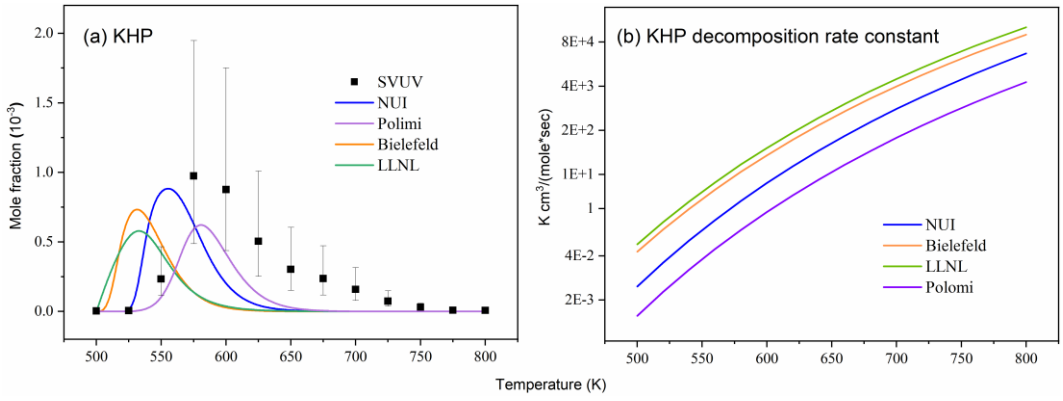

Fig. 2: Measured mole fraction profile of C7 KHP (symbol) by SVUV-PIMS in JSR-1 and modeling results using different mechanisms, including NUI [15], LLNL [17], Polimi [40] and Bielefeld models [47]. Rate constant of KHP decomposition used in all models is also presented. KHP mole fraction uncertainty is estimated at a factor of two.

Figure 3 shows a comparison of the experimental results of *n*-heptane, O_2, and C7 KHP with prediction by the following models, the NUI model (dashed line), the NUI model with a second O_2 addition rate constant increased by a factor of two (NUI model-1, dash dotted line), and the NUI model with a second O_2 addition rate constant increased by a factor of two, the C7 KHP decomposition rate constant was reduced, and the C7 keto-alkoxyl radical decomposed to C3-C6 diones (NUI model-2, solid line). It can be seen that NUI model-2 predicted the consumption of *n*-heptane and O_2 well, as well as the temperature dependence of C7 KHP.

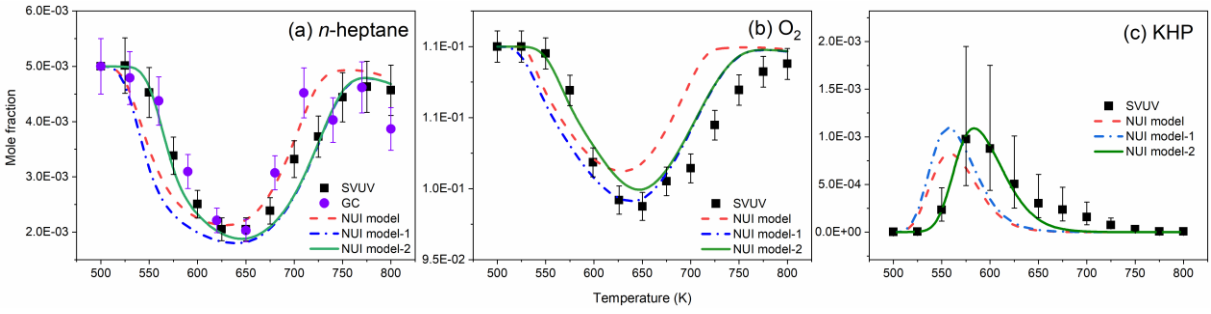

Fig. 3: Experimental (symbols) and modeling results (lines) for mole fraction of (a) *n*-heptane by SVUV-PIMS in JSR-1 and GC in JSR-2, (b) O_2 by SVUV-PIMS in JSR-1, and (c) C7 KHP by SVUV-PIMS in JSR-1during the JSR oxidation of *n*-heptane. Dashed line represents simulation by

NUI model, dashed dotted line by NUI model-1, and solid line by NUI model-2. (Description of models found in the text.) Uncertainty in *n*-heptane and O_2 mole fraction ± 10%; uncertainty on KHP mole fraction estimated at a factor of two.

As previously discussed, increasing the rate constant of the second O_2 addition promoted the formation of •OOQOOH radical, accelerating the generation of C7 KHP. Additional OH radicals were then produced via chain branching reactions, which promoted *n*-heptane low temperature oxidation reactivity (dash dotted line). However, in NUI model-2 the rate constant of C7 KHP decomposition was reduced, thereby also reducing the formation of OH radicals. A new balance for the formation of OH radicals was achieved, which predicted the experimental observation well. Because the low temperature oxidation mechanism was very complex and not fully understood and the reaction kinetics were based on limited experimental measurements and quantum chemistry calculations, a probable solution in this work that used different rate rules for the second O_2 addition and for C7 KHP decomposition could also predict the low temperature oxidation of *n*-heptane.

3.3 Korcek reaction of C7 KHP

It was commonly recognized that carbonyl acid is generated mainly through the oxidation of aldehydes and the Baeyer-Villiger reaction [48, 49]. However, Korcek *et al*. [50, 51] conducted a detailed analysis of the oxidation products of *n*-hexadecane autoxidation process in the last century and found that those pathways alone could not account for the formation of the measured acids. Moreover, they proposed [52] that the carboxylic acids could be formed from γ-KHP decomposition (i.e., the Korcek mechanism). Recently, Jalan *et al*. [48] used theoretical calculations to study the decomposition of γ-KHP, and investigated the two basic pathways of the Korcek reaction. Their studies showed that KHP not only generated OH radicals through direct decomposition, but may also undergo isomerization and decompose into acids via the Korcek reaction.

In this work, C1-C4 carboxylic acids (i.e., formic acid, acetic acid, propionic acid, and butyric acid) were measured by the SVUV-PIMS. Formic acid and acetic acid were also measured by FTIR

in the JSR experiment at Orléans, but the measured mole fraction was higher than that measured by SVUV-PIMS. The source of the discrepancies were not clear. It was noted that the mole fraction in propionic and butyric acid may include the contribution of C3 and C4 olefinic hydroperoxides, therefore we estimated that the mole fraction of propionic acid and butyric acid measured by SVUV-PIMS had an uncertainty of ± 50%. In the NUI model, the Korcek reactions from C7 KHP to formic, acetic, and propionic acids were included. For formic acid, the addition reaction of OH radical to formaldehyde/acetaldehyde, and the following dehydrogenation/dealkylation could also lead to its formation. However, the rate constants used were much higher than the experiment measurement and theoretical calculation [29, 53, 54]. The dashed lines in Fig. 4 are the prediction of the C1-C4 carboxylic acids by the NUI model. The mole fraction of the formic acid was significantly over-predicted, while that for C2-C3 carboxylic acids was significantly under-predicted, and there was no prediction for the butyric acid because there were no reactions for butyric acid in the NUI model.

The solid lines in Fig. 4 are the prediction of C1-C4 carboxylic acids by the *NUI model-3*, developed by adding the Korcek reactions of C7 KHP to NUI model-2. One reaction pathway was added for C7 KHP to butyric acid in NUI model-3. Furthermore, the rate constant OH radical to formaldehyde was updated from the calculations of Xu *et al*. [29]. The rate constant OH radical to acetaldehyde was estimated from OH radical addition to formaldehyde. Due to the rate constant reduction of C7 KHP decomposition, the Korcek reaction became relatively important and more carbon flux went to the carboxylic acids. It can be seen that the prediction for these acids was significantly improved, especially for C2-C4 carboxylic acids. However, the mole fraction of formic acid was notably under-predicted, even after the Korcek reaction was considered in the model.

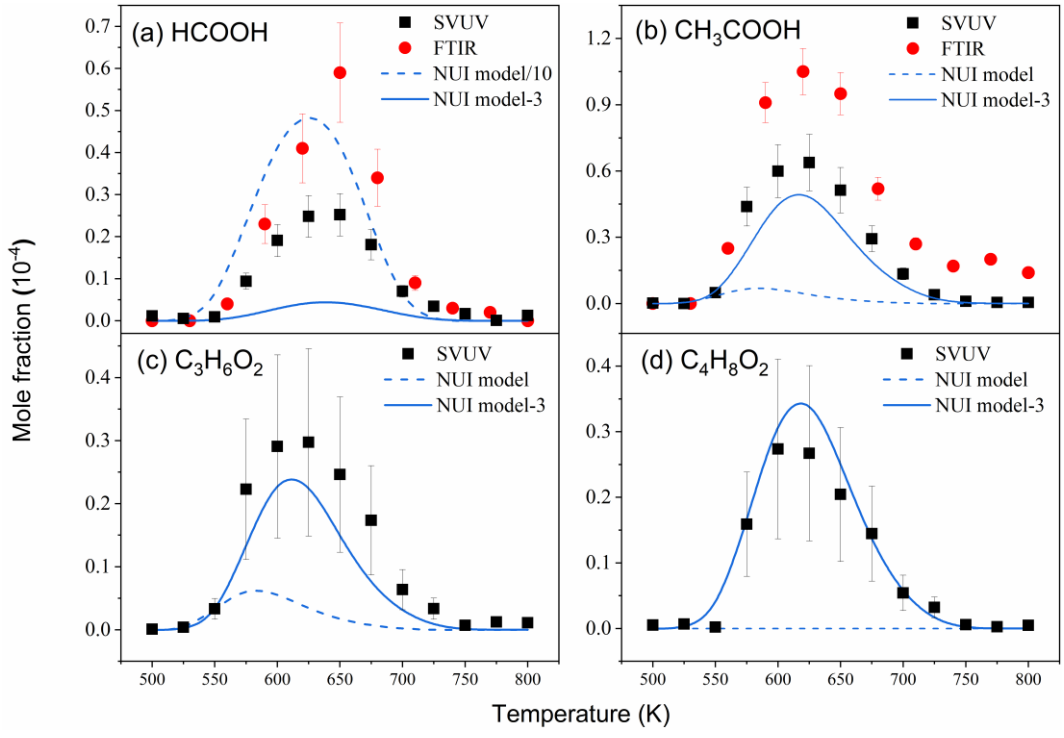

Fig. 4: Experimental (symbols) and simulation (line) results of carbonyl acid during JSR oxidation of *n*-heptane. Black squares represent SVUV-PIMS data in JSR-1; red circles are FTIR data in JSR-2. Dashed lines are simulations from NUI model; solid line is simulations by NUI model-3. (Model description found in the text.). Uncertainty of mole fraction of formic and acetic acid is ± 20%, and uncertainty of mole fraction of propionic acid and butyric acid is estimated at ± 50% for SVUV-PIMS measurement. In the case of formic acid and acetic acid measured by FTIR, error bars could be as high as +/- 10 ppm.

3.4 H-abstraction on C7 KHP

Because of the weak O-OH bond of the hydroperoxyl group in KHP, the hydroperoxyl group easily broke into OH and keto-alkoxy radicals. However, in the previous alkane low-temperature oxidation mechanism, KHP consumption proceeded by breaking the O-O bond, and the H-abstraction of KHP reaction was seldom considered in the kinetic models [40]. Recent work by Xing *et al*. [30] showed that, in addition to breaking the O-O bond, KHP may also undergo H-abstraction reaction to generate different products, such as diones, keto cyclic ethers or olefinic ketones. These products were detected experimentally in the present work. So, the H-abstraction reaction of KHP

may play an important role during alkane low temperature oxidation. In this study, the rate constants of H-abstraction on C7 KHPs by the OH radical to produce C7 KHP radicals were added to NUI model-3, in reference to the theoretical calculation of Xing *et al*. [30] on 4-hydroperoxy-2-pentanone. Subsequently, C7 KHP radicals underwent β-scission, concerted elimination, or cyclization, to produce these products. The kinetic model that considered H-abstraction reactions on C7 KHP, and the subsequent reactions of the C7 KHP radicals is named *NUI model-4*. Here, 4-hydroperoxy-2-heptanone was used as an example to illustrate the reaction network of C7 KHP + OH reactions (Scheme 2).

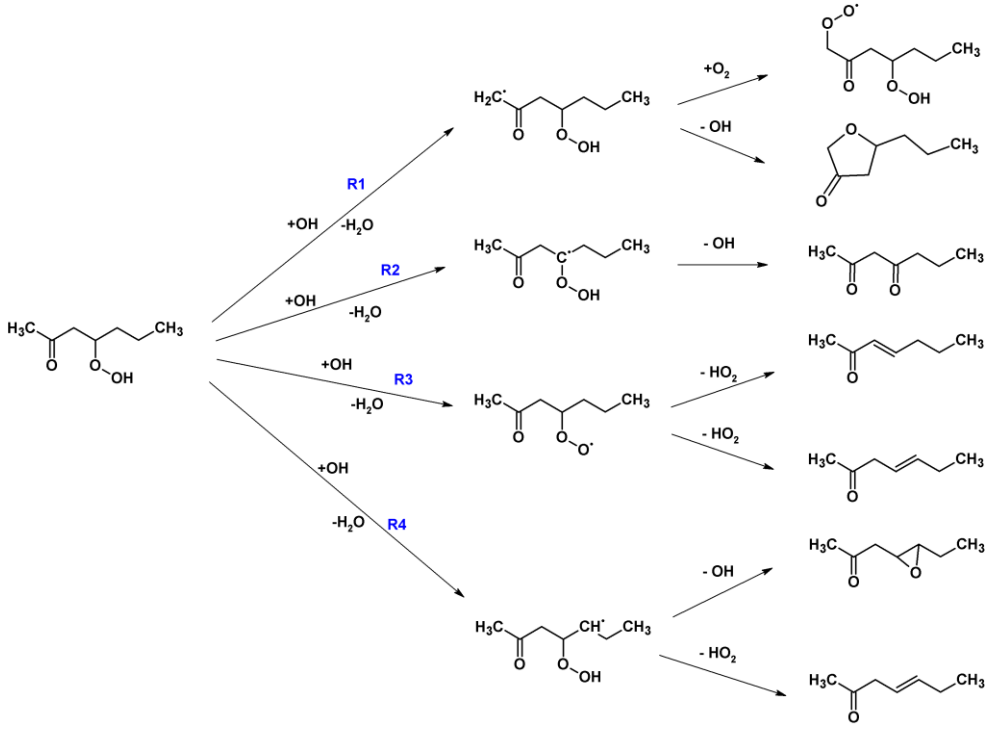

Scheme 2: Reaction pathways for H-abstraction reaction from 4-hydroperoxy-2-heptanone by OH radicals. Here, we only present some typical reaction channels to illustrate the reaction mechanism.

The H-abstraction reaction at various sites on KHP led to the formation of various products. The four channels presented in Scheme 2 are addressed next. When the H atom was abstracted at the β-site of a carbonyl group (for example R1 in Scheme 2), the KHP radical could undergo O_2 addition reaction to generate a peroxide KHP radical, or cyclize to form a keto cyclic ether and OH radical.

The rate constant for the β-scission reaction was based on the recommendations of Bugler *et al*. [55], and the rate constant for the formation of a keto cyclic ether is analogous to that for a cyclic ether formation reaction [15, 32] with the same ring size. For the H atom on the carbon atom where the -OOH group was located, the radical formed after H-abstraction became unstable (R2) and immediately decomposed into a dione and an OH radical. Therefore, for this H-abstraction reaction, the KHP radical transition state was omitted, and dione, OH radical and H_2O were directly produced with a lumped description. Because the variational effects and multistructural torsional anharmonicity play an important role in KHP, the H-abstraction of the H atom from the hydroperoxy group (R3) was the dominant H-abstraction reaction, although R2 had the lowest energy barrier [30]. After the H atom was abstracted from the -OOH group, a ketoalkylperoxy radical is formed. The further loss of a HO_2 radical from the ketoalkylperoxy radical forms the heptenone. We note that ketoalkylperoxy radical from R3 could undergo dissociation reaction to form O_2 and the heptanone radical. This reaction was not included in the model. Reaction (R4) was the H-abstraction reaction on the CH_2 group in β of the hydroperoxy group. The radical produced in β to the hydroperoxy group could decompose into heptenone or undergo cyclization to produce a keto cyclic ether. The rate constants for the H-abstraction reactions were estimated from the calculation of Xing *et al*. [30], or for molecules with similar structure. Reaction rate constants of the C7 KHP radical reactions were estimated from alkyl peroxy radical (ROO•) and •QOOH radicals with similar structures. These estimations are documented as comments in the Chemkin mechanism file. It was considered that the analogies were reasonable to explore the reaction mechanism of the C7 KHP. However, further experimental measurements and/or theoretical calculations of the rate constants would help reduce the uncertainties of the prediction.

Mole fraction profiles of $C_7H_{12}O$ and $C_7H_{12}O_2$ measured by SVUV-PIMS are presented in Fig. 5. As discussed above, these two C7 products produced in *n*-heptane oxidation process consist of

large number of isomers, and it was difficult to probe all isomers and measure their mole fractions. However, these different isomers should have similar ionization properties because their chemical structures are similar. Therefore, in the calculation of the mole fractions of $C_7H_{12}O$, it was assumed to be heptenones, while $C_7H_{12}O_2$ was assumed to be heptadiones. To quantify these two intermediates, 3-hepten-2-one and 3,5-heptanedione were adopted as the model compounds for heptenones and heptadiones, respectively. The measured PICS of 3-hepten-2-one and 3,5-heptanedione are shown in Fig. S1 in the Supplementary Material. In NUI model-4, the H-abstraction reactions on C7 KHP were included, the heptenones ($C_7H_{12}O$) could be formed, and heptadiones and keto cyclic ethers ($C_7H_{12}O_2$) could be produced. As shown in Fig. 5, the computed mole fractions of heptenones from C7 KHP (dashed line) were close to the experimental measurement; they were formed in the temperature range of 500-650 K. Similar results were observed for heptadiones (dashed dotted dotted line) and keto cyclic ethers (dashed line) formed from C7 KHP, compared with the experimental measurements of the mole fraction of $C_7H_{12}O_2$ (Fig. 5b). The results showed that the H-abstraction on C7 KHP could explain the formation of $C_7H_{12}O$ and $C_7H_{12}O_2$ from 500-650 K, but there were still large differences between the model prediction and the experimental measurements in the temperature range between 650-750 K. Therefore, other pathways must sustain the formation of $C_7H_{12}O$ and $C_7H_{12}O_2$ intermediates, for example the reaction of cyclic ethers and heptenes, which were formed at relatively higher temperature than the C7 KHPs. These reactions are discussed next.

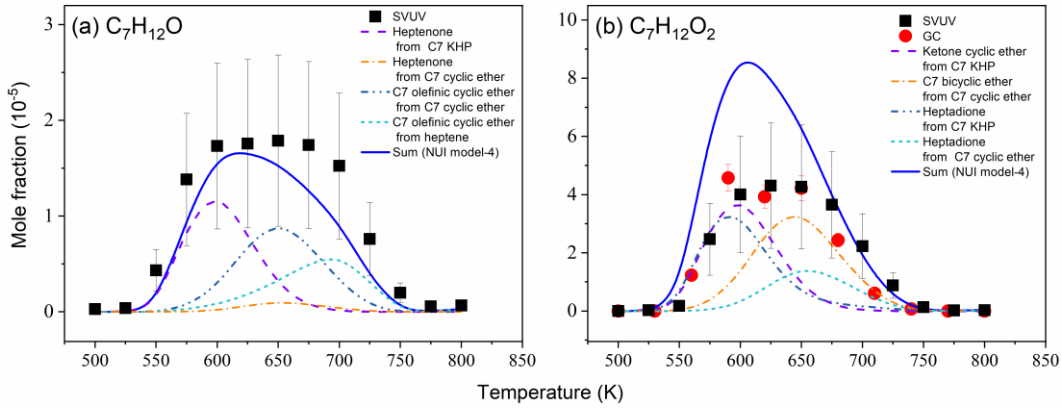

Fig. 5: Experimental (symbols) and simulation (line) results of $C_7H_{12}O$ and $C_7H_{12}O_2$ during JSR oxidation of *n*-heptane. Black squares represent SVUV-PIMS data in JSR-1; red circles are GC data in JSR-2. Simulated mole fractions of $C_7H_{12}O$ and $C_7H_{12}O_2$ formed from reactions of C7 KHP, cyclic ether, and heptene are presented. Mole fraction uncertainty of $C_7H_{12}O$ and $C_7H_{12}O_2$ estimated at ± 50%.

3.5 C7 cyclic ether and heptene oxidation

During the low temperature oxidation of *n*-heptane, C7 cyclic ethers were the main products produced through cyclization reaction from hydroperoxyl alkyl radicals (•QOOH). This was the chain propagation reaction, which competed with the chain branching reaction that controlled the low temperature oxidation reactivity. The consumption pathways of cyclic ethers were not well established in the *n*-heptane kinetic models [10], where they underwent H-abstraction reactions by OH radicals, and decomposed into small molecules via a ring-opening of cyclic ether radicals. Recently, there have been studies on low temperature oxidation of cyclic ethers, and detailed reaction mechanisms for cyclic ethers oxidation were developed. This work considered the O_2 addition reaction to the cyclic ether radicals and their subsequent reactions. The reaction mechanism was analogous to the 2,5-dimethyl-tetrahydrofuran mechanism proposed by Fenard *et al.* [36].

Scheme 3 shows the reaction pathways of 2-ethyl-5-methyl-tetrahydrofuran, the dominant cyclic ether isomer formed during *n*-heptane low temperature oxidation. The H-abstraction of 2-ethyl-5-methyl-tetrahydrofuran formed seven cyclic ether radicals; only reaction pathways yielding

$C_7H_{12}O$ and $C_7H_{12}O_2$ intermediates are shown here. O_2 addition to the radical site formed ROO• -type radicals. Concerted elimination of the ROO• radical formed olefinic cyclic ethers, while the intramolecular H-migration via five, six and seven membered-ring transition states formed •QOOH radicals, which further lead to the formation of heptenones, heptadiones and C7 bicyclic ethers.

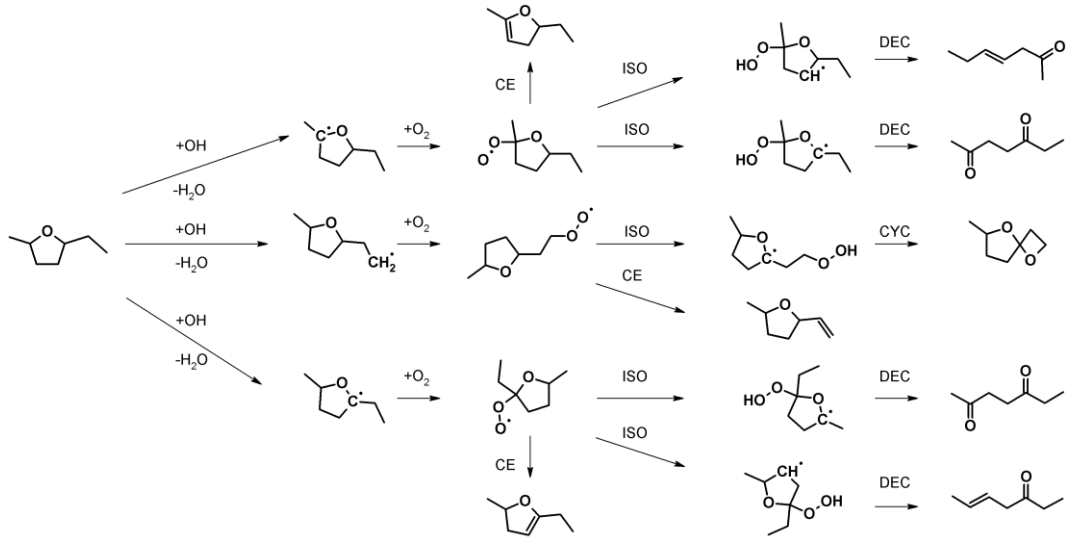

Scheme 3: Low temperature oxidation pathway of 2-ethyl-5-methyl-tetrahydrofuran which formed heptenones, heptanediones, and C7 bicyclic ether. Second O_2 addition to •QOOH radical not presented in figure. ISO: isomerization, CE: concerted elimination, CYC: cyclic ether formation reaction, DEC: decomposition reaction. Here, we only present some typical reaction channels to illustrate the reaction mechanism.

This work also considered the low temperature oxidation reaction of the heptenes. The reaction mechanism of heptenes was similar to that of the alkanes if the H-abstraction was on the primary and secondary C-Hs. The cyclization of the •QOOH radicals could form olefinic cyclic ethers, one of the $C_7H_{12}O$ isomers.

After considering the oxidation reaction of cyclic ethers and heptenes, the model was named *the NUI model-5*. The simulated mole fractions of $C_7H_{12}O$ olefinic cyclic ethers (dash dotted dotted line, dotted line), $C_7H_{12}O_2$ heptadiones (dotted line) and bicyclic ethers (dashed dotted line) are shown in Fig. 5. It can be seen that these $C_7H_{12}O$ and $C_7H_{12}O_2$ intermediates formed from the C7

cyclic ethers and heptene oxidation had a maximum mole fraction at 650 K, which is expectedly ca. 50 K higher than the $C_7H_{12}O$ and $C_7H_{12}O_2$ intermediates formed from C7 KHP. The simulated mole fractions of the heptenones (dashed dotted line) formed from C7 cyclic ether oxidation were very weak. The sum of the computed mole fraction profiles of the $C_7H_{12}O$ and $C_7H_{12}O_2$ isomers, formed from H-abstraction on KHPs, the oxidation of cyclic ethers, and the oxidation of heptenes, predicted the measured temperature-dependent profiles of $C_7H_{12}O$ and $C_7H_{12}O_2$ well. The predicted total mole fractions of $C_7H_{12}O$ also agreed well with the experimental measurements. The prediction of the mole fractions of $C_7H_{12}O_2$ was also acceptable, considering the uncertainties from the experiment and model development and related assumptions.

3.6 C3-C6 diones reactions

The C3-C6 diones in this work were measured using SVUV-PIMS. The PICS of 2,3-butanedione, 2,3-pentanedione, and 2,5-hexanedione (Fig. S1), were measured and used to calculate the mole fractions of the C4-C6 diones. The measured PIE curves of the $C_4H_6O_2$, $C_5H_8O_2$, $C_6H_{10}O_2$ species agree with the PICS curve of 2,3-butanedione, 2,3-pentanedione, and 2,5-hexanedione. For $C_3H_4O_2$, the measured ionization energy is in good agreement with that of 2,3-butanedione, indicating that $C_3H_4O_2$ could also be diones. The PICS of C3 diones was estimated to be 5 Mb at 9.5 eV by analyzing the PICS of 2,3-butanedione, 2,3-pentanedione, and 2,5-hexanedione. Here, we estimated the mole fraction uncertainty of the C3-C6 diones at ± 50%. The mole fraction profiles of the C3-C6 diones are shown in Fig. 6. The original NUI model did not include reactions to the C3-C6 diones, so there was no prediction for their formation. As mentioned in section 3.2, NUI model-2 included C3-C6 diones formation pathways from the decomposition of C7 KHP via formation of the keto-alkoxyl radicals. The dashed lines in Fig. 6 are simulation results for C3-C6 diones from C7 KHP decomposition. Except for C6 diones, the formation of C3-C5 diones from C7 KHP was lower than the experiment measurements. In addition to C7 KHP decomposition, there are other pathways

for the formation of C3-C5 diones. In NUI model-5, the low temperature oxidation of cyclic ethers also led to the formation of bicyclic ether hydroperoxides ($C_7H_{12}O_4$), which underwent decomposition and could also form C3-C5 diones. The dashed dotted lines in Fig. 6 are simulated mole fractions of C3-C6 diones formed from the decomposition of bicyclic ether hydroperoxides. The solid lines are the total mole fraction of C3-C6 diones from the decomposition of C7 KHP and the decomposition of bicyclic ether hydroperoxides. It can be seen that NUI model-5 predicted the mole fraction profiles of C3-C5 diones well, while over-predicting the mole fraction profile of C6 diones.

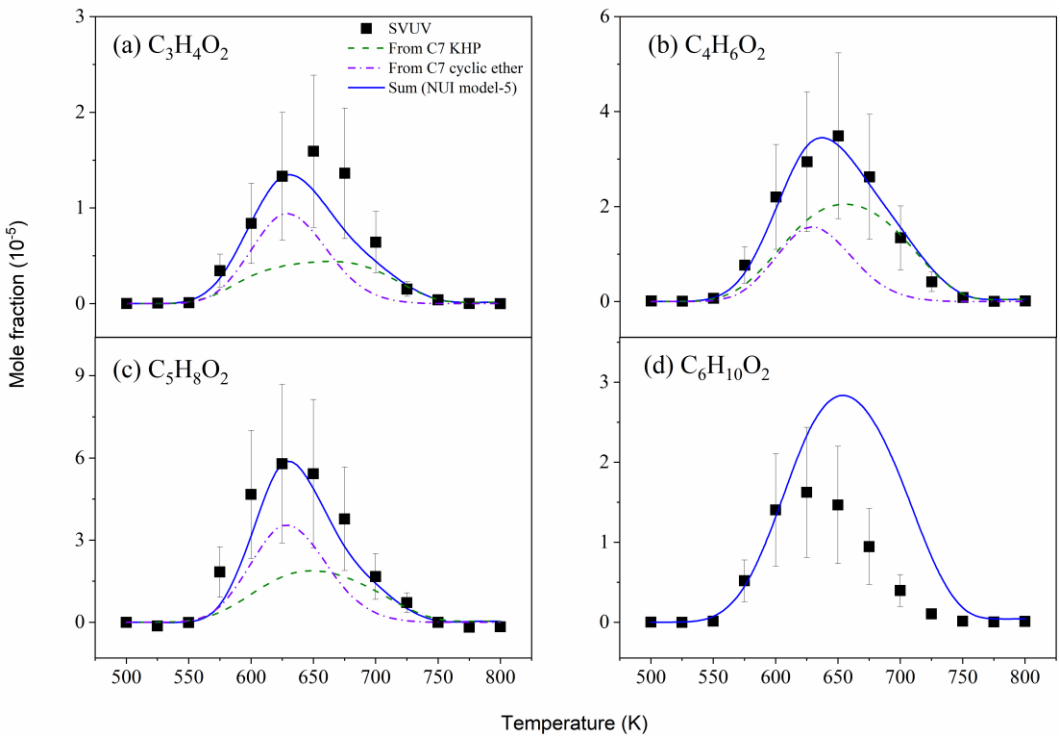

Fig. 6: Experimental (symbols) and simulation (line) results of C3-C6 diones during JSR oxidation of *n*-heptane. Black squares represent SVUV-PIMS data in JSR-1. Mole fraction uncertainty of the C3-C6 diones estimated at ± 50%. Simulated mole fractions of C3-C6 diones from decomposition of C7 KHP and bicyclic ether hydroperoxides presented.

3.7 Third O_2 addition reactions

Wang *et al*. [16] proposed the third O_2 addition reactions and found that including them in kinetic models promoted low temperature reactivity and shortened ignition delay time, especially under high pressure conditions. In this work, we included the third O_2 addition reactions into NUI model-5; the model with the third O_2 addition reactions is named *NUI model-6*. Details on the mechanism development are in Ref. [16].

As shown in Scheme. 1, the reactions began with •P(OOH)$_2$ radicals, which added to O_2 and formed •OOP(OOH)$_2$ radicals. Subsequently, the isomerization of •OOP(OOH)$_2$ formed keto-di-hydroperoxides (KDHP) and an OH radical, or isomerized to a •T(OOH)$_3$ radical, which underwent a cyclization reaction, forming di-hydroperoxy cyclic ether (DHPCE) and an OH radical. Both are important isomers of $C_7H_{14}O_5$. Figure 7a shows the experimentally measured signal and the model predicted mole fraction of $C_7H_{14}O_5$. It can be seen that the NUI model-6 captured the temperature-dependent profile of $C_7H_{14}O_5$ well. Simulation revealed that KDHP was the dominant component of $C_7H_{14}O_5$. The model simulated mole fraction of $C_7H_{12}O_4$ and the experimentally measured signal profile of $C_7H_{12}O_4$ are shown in Fig. 7b. The composition of $C_7H_{12}O_4$ is relatively complicated; it is composed of three kinds of isomers: cyclic ether ketone-hydroperoxide (CEKHP), diketone-hydroperoxide (DKHP), and bicyclic ether hydroperoxide (BCEHP). CEKHP and DKHP could be derived from the oxygen addition to the KHP radical, followed by subsequent intramolecular H-abstraction, and then followed by cyclization/decomposition. BCEHP could be formed from the oxidation process of cyclic ether.

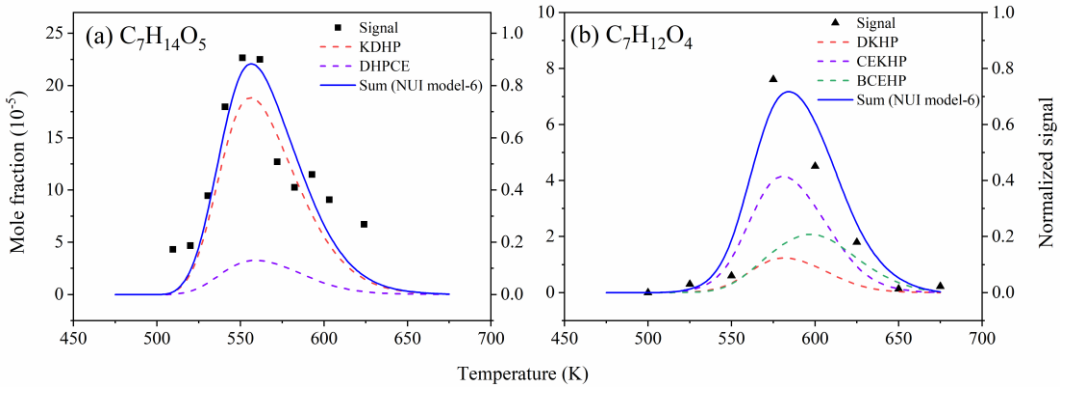

Fig. 7: Experimental (symbols) and simulation results (line) of $C_7H_{14}O_5$ and $C_7H_{12}O_4$ during *n*-heptane low temperature oxidation. Black squares in (a) represent SVUV-PIMS data for stoichiometric *n*-heptane (1%)/O_2 (11%)/Ar (78%) at quasi-atmospheric pressures of 0.933 bar and residence time of 2s from Ref. [7]. Recorded reactor temperature corrected according to Ref. [44]. Black triangles in (b) are SVUV-PIMS data measured in JSR-1. Simulated mole fractions of probable $C_7H_{14}O_5$ and $C_7H_{12}O_4$ isomers presented.

The effect of the third O_2 addition reaction on the low temperature oxidation of *n*-heptane in JSR at 1 bar, and on the IDT of *n*-heptane at 20 and 40 bar appears in Fig. 8. It can be seen that for the JSR low temperature oxidation at 1 bar, both the model *without* the third O_2 addition reactions (NUI model-5) and *with* the third O_2 addition reactions (NUI model-6) predicted the mole fraction profiles of *n*-heptane and O_2 well. The third O_2 addition reactions slightly promoted the reactivity of *n*-heptane oxidation from 500 to 650 K, but there was no influence on the reactivity of the negative temperature coefficient (NTC) zone (650-800 K). Although NUI model-5 predicted the low temperature oxidation reactivity of *n*-heptane at 1 bar well, it under-predicted the IDT of *n*-heptane at high pressures of 20 and 40 bar, and in the temperature range between 600-673 K. IDT predicted by NUI model-6, including the third O_2 addition reactions, agreed well with the experimentally measured IDT of *n*-heptane oxidation. It was observed that the promoting effect of the third O_2 addition reactions on low temperature oxidation reactivity was more pronounced at high pressures.

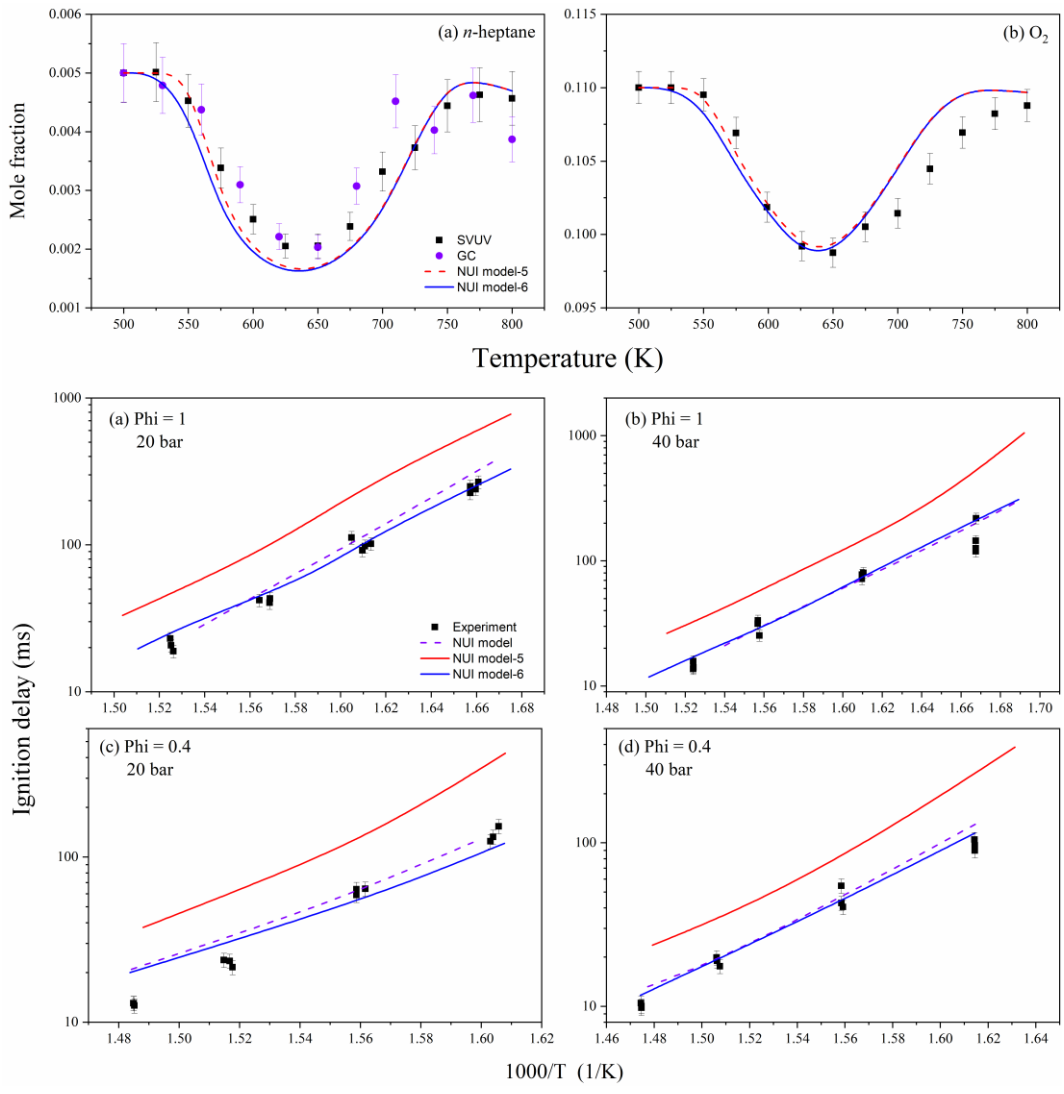

Fig. 8: Effect of third O_2 addition reactions on prediction of *n*-heptane low temperature oxidation in JSR at 1 bar, and on IDT of *n*-heptane/O_2/CO_2 mixtures at 20 and 40 bar.

3.8 Overview of the reaction pathways

Based on the discussion in Section 3.1-3.7, a more comprehensive kinetic model was developed for *n*-heptane low temperature oxidation. As shown in Figs. S2-S5, the final oxidation products (hydrocarbon and oxygenated intermediates during JSR oxidation of *n*-heptane) were predicted well by the kinetic model. The kinetic model was also validated against the IDT of *n*-heptane under other experimental conditions, as shown in Figs. S6-S7. Generally, the model satisfactorily predicted the IDT, except for a slight over-prediction of IDT in the NTC zone (Fig. S6).

These results indicated that the reaction mechanism developed for *n*-heptane was reasonable. A kinetic analysis revealed that the second O_2 addition, the decomposition of C7 KHP, and the third O_2 addition reactions influenced the low temperature oxidation reactivity of *n*-heptane. These reactions controlled the formation of OH radicals. Compared to the original NUI model, the promoting effect of the second O_2 addition, the reduction of the C7 KHP decomposition rate, and the inclusion of the third O_2 addition reactions promoted a new balance for OH formation, which in turn gave a good prediction of speciation data for *n*-heptane low temperature oxidation at 1 bar, and the IDT of *n*-heptane at higher pressures. The H-abstraction of C7 KHP, the Korcek reactions of C7 KHP, the decomposition of the C7 keto-alkoxyl radicals, and the low temperature reactions of the cyclic ethers and heptenes had little effect on the low temperature oxidation reactivity of *n*-heptane, but these reactions explained the formation of $C_7H_{12}O$ and $C_7H_{12}O_2$ intermediates, carboxyl acids, and C3-C6 diones.

The rate of production (ROP) analysis at 1 bar and 575 K for *n*-heptane oxidation in JSR is shown in Fig. 9. Here we only show one ROO• isomerization pathway, and the subsequent reactions of one •QOOH radical. We note that the ROP analysis is not to give a detailed analysis of the reaction pathways. It gives a general picture of the low-temperature reaction network of *n*-heptane that was improved by completing the reaction mechanism, including the reactions of heptene, keto-hydroperoxide, cyclic ether and third oxygen addition reactions. The sensitivity analysis of the IDT in RCM experiment and of *n*-heptane and O_2 in JSR experiment are presented in Figs. S8-S9.

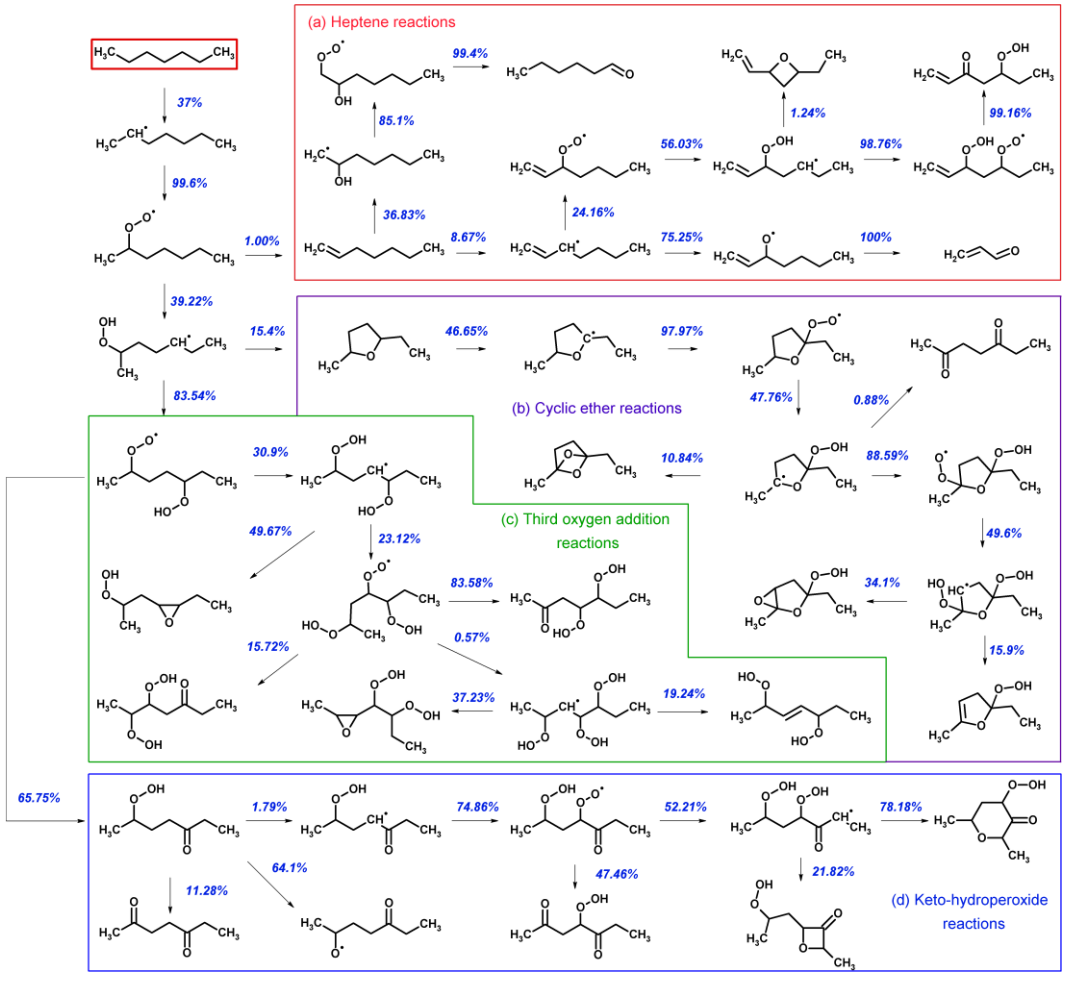

Fig. 9: Reaction flux for *n*-heptane oxidation in JSR at a temperature of 575 K, p = 1 bar, 0.5% fuel in argon, τ = 1 s, ϕ = 0.5. The reaction classes are separated as (a) heptene reactions; (b) cyclic ether reactions; (c) third oxygen addition reactions and (d) keto-hydroperoxide reactions, respectively. Here we only show one ROO• isomerization pathway, and the subsequent reactions of one •QOOH radical. We note that not all reactions are presented.

4. Summary and conclusions

In this work, the low temperature oxidation of *n*-heptane in a jet-stirred reactor at 1 bar was investigated using SVUV-PIMS and GC/FTIR analysis. New ignition delay time data of *n*-heptane/O_2/CO_2 mixtures were measured in a rapid compression machine. Using CO_2 as the dilution gas allowed the reaction temperature to approach as low as 600 K. A more detailed kinetic mechanism of *n*-heptane oxidation was developed by adding the sub-mechanism of C7 keto-

hydroperoxides, C7 cyclic ethers and heptene isomers, and by evaluating the rate constant of C7 KHP decomposition and the second O_2 addition reactions. Moreover, the third O_2 addition reactions of *n*-heptane low temperature oxidation was also included in the kinetic model. Overall, the newly proposed *n*-heptane kinetic model in this work reasonably predicted the experimental observations. The main conclusions of this work are as follows:

(1) The current kinetic model increased the rate constant of the second O_2 addition reaction, which led to better prediction of oxygen consumption. The reduction of the decomposition rate constant of C7 KHP led to better prediction of the temperature dependence of C7 KHP and the low temperature oxidation reactivity of *n*-heptane at 500-650 K. The third O_2 addition reactions had a more obvious influence on the low temperature oxidation reactivity of *n*-heptane, as in ignition delay times at 20 and 40 bar. These three reaction classes influenced the formation of OH radicals, and subsequently, the prediction of low temperature oxidation reactivity and speciations as a function of temperature.

(2) The current kinetic model gave a better prediction for C7 oxidation products like $C_7H_{12}O$ and $C_7H_{12}O_2$ because the bimolecular reaction of C7 KHP with OH radicals were considered, as well as low temperature reactions of C7 cyclic ethers and heptenes in the model. Simulations showed that two main components for $C_7H_{12}O$, i.e., heptenones from H-abstraction on KHP, and olefinic cyclic ethers from C7 cyclic ethers and heptenes oxidation. $C_7H_{12}O_2$ contained mainly keto cyclic ethers obtained from H-abstraction on C7 KHP, diones from H-abstraction on C7 KHP and C7 cyclic ethers oxidation, and bicyclic ethers from C7 cyclic ethers oxidation. Previous work usually regarded the $C_7H_{12}O_2$ intermediates as diones, formed from KHP. Our experimental measurements, and the kinetic model predictions, indicated that other isomers, such as keto cyclic ethers and bicyclic ethers were also important fractions of $C_7H_{12}O_2$. This work shows that both C7 KHPs and cyclic ethers form $C_7H_{12}O_2$, but the different $C_7H_{12}O_2$ intermediates have different temperature-dependent profiles.

(3) The Korcek reaction of C7 KHP that led to carboxylic acids became more important when the rate constant of C7 KHP decomposition was reduced. Results showed that even if the Korcek reaction was included in the model, and the rate constant of C7 KHP decomposition was reduced, the model significantly under-predicted the mole fraction of formic acid. The formation pathways for formic acid are still unclear.

(4) C3-C6 diones were measured by SVUV-PIMS. Their formation could be explained from the decomposition of the C7 KHP, and the decomposition of the bicyclic hydroperoxides which were formed through the low temperature oxidation of C7 cyclic ethers.

During this work, not only predictions of key species like O_2, C7 KHP, C7 oxidation products, C2-C4 carboxylic acids, and C3-C6 diones significantly improved, but the ignition delay time of *n*-heptane/O_2 mixtures over wide experimental conditions was also captured well. This study provides new insight into the understanding of the low temperature oxidation mechanism of *n*-heptane. Future work could adopt this methodology to evaluate the kinetic models of other alkanes, and consider the reaction mechanism of highly oxygenated molecules (HOMs) formation in the models.

Acknowledgements

This work was supported by the National Natural Science Foundation of China (51976208), by Hefei Science Center, CAS (2020HSC-KPRD001), and by the DNL Cooperation Fund, CAS (DNL202005). The work of KAUST authors was funded by the Office of Sponsored Research (OSR) at King Abdullah University of Science and Technology (Grant CRG2020-URF-1435). Work at CNRS Orléans received funding from the Labex Caprysses (ANR-11-LABX-0006-01) and from the Région Centre Val de Loire, EFRD, and CPER (projects PROMESTOCK and APROPOR-E).

References

[1] B. Niu, X. Yu, Z. Shen, Structure Adjustment of Automobile Supply Chain Facing Low-carbon Emission Standard, Resour. Conserv. Recycl. 171 (2021) 105629.

[2] J.E. Dec, Advanced compression-ignition engines-understanding the in-cylinder processes, Proc. Combust. Inst. 32 (2009) 2727-2742.
[3] J. Zádor, C.A. Taatjes, R.X. Fernandes, Kinetics of elementary reactions in low-temperature autoignition chemistry, Prog. Energy Combust. Sci. 37 (2011) 371-421.
[4] S.M. Sarathy, A. Farooq, G.T. Kalghatgi, Recent progress in gasoline surrogate fuels, Prog. Energy Combust. Sci. 65 (2018) 67-108.
[5] S.M. Sarathy, G. Kukkadapu, M. Mehl, W.J. Wang, T. Javed, S. Park, M.A. Oehlschlaeger, A. Farooq, W.J. Pitz, C.J. Sung, Ignition of alkane-rich FACE gasoline fuels and their surrogate mixtures, Proc. Combust. Inst. 35 (2015) 249-257.
[6] S.M. Sarathy, E.A. Tingas, E.F. Nasir, A. Detogni, Z.D. Wang, A. Farooq, H. Im, Three-stage heat release in n-heptane auto-ignition, Proc. Combust. Inst. 37 (2019) 485-492.
[7] Z.D. Wang, B.J. Chen, K. Mosharnmer, D.M. Popolan-Vaida, S. Sioud, V.S.B. Shankar, D. Vuilleumier, T. Tao, L. Ruwe, E. Brauer, N. Hansen, P. Dagaut, K. Kohse-Höinghaus, M.A. Raji, S.M. Sarathy, n-Heptane cool flame chemistry: Unraveling intermediate species measured in a stirred reactor and motored engine, Combust. Flame 187 (2018) 199-216.
[8] C.M. Coats, A. Williams, Investigation of the ignition and combustion of n-heptane-oxygen mixtures, Symp. (Int.) Combust. 17 (1979) 611-621.
[9] C.K. Westbrook, J. Warnatz, W.J. Pitz, A detailed chemical kinetic reaction mechanism for the oxidation of iso-octane and n-heptane over an extended temperature range and its application to analysis of engine knock, Symp. (Int.) Combust. 22 (1989) 893-901.
[10] H.J. Curran, P. Gaffuri, W.J. Pitz, C.K. Westbrook, A comprehensive modeling study of n-heptane oxidation, Combust. Flame 114 (1998) 149-177.
[11] E. Ranzi, T. Faravelli, P. Gaffuri, A. Sogaro, Low-temperature combustion: Automatic generation of primary oxidation reactions and lumping procedures, Combust. Flame 102 (1995) 179-192.
[12] O. Herbinet, B. Husson, Z. Serinyel, M. Cord, V. Warth, R. Fournet, P.A. Glaude, B. Sirjean, F. Battin-Leclerc, Z.D. Wang, M.F. Xie, Z.J. Cheng, F. Qi, Experimental and modeling investigation of the low-temperature oxidation of n-heptane, Combust. Flame 159 (2012) 3455-3471.
[13] A. Rodriguez, O. Herbinet, X. Meng, C. Fittschen, Z. Wang, L. Xing, L. Zhang, F. Battin-Leclerc, Hydroperoxide Measurements During Low-Temperature Gas-Phase Oxidation of n-Heptane and n-Decane, J. Phys. Chem. A. 121 (2017) 1861-1876.
[14] E. Ranzi, C. Cavallotti, A. Cuoci, A. Frassoldati, M. Pelucchi, T. Faravelli, New reaction classes in the kinetic modeling of low temperature oxidation of n-alkanes, Combust. Flame 162 (2015) 1679-1691.
[15] K.W. Zhang, C. Banyon, J. Bugler, H.J. Curran, A. Rodriguez, O. Herbinet, F. Battin-Leclerc, C. B'Chir, K.A. Heufer, An updated experimental and kinetic modeling study of n-heptane oxidation, Combust. Flame 172 (2016) 116-135.
[16] Z.D. Wang, D.M. Popolan-Vaida, B.J. Chen, K. Moshammer, S.Y. Mohamed, H. Wang, S. Sioud, M.A. Raji, K. Kohse-Höinghaus, N. Hansen, P. Dagaut, S.R. Leone, S.M. Sarathy, Unraveling the structure and chemical mechanisms of highly oxygenated intermediates in oxidation of organic compounds, Proc. Natl. Acad. Sci. U.S.A. 114 (2017) 13102-13107.
[17] S.M. Sarathy, C.K. Westbrook, M. Mehl, W.J. Pitz, C. Togbe, P. Dagaut, H. Wang, M.A. Oehlschlaeger, U. Niemann, K. Seshadri, P.S. Veloo, C. Ji, F.N. Egolfopoulos, T. Lu,

Comprehensive chemical kinetic modeling of the oxidation of 2-methylalkanes from C_7 to C_{20}, Combust. Flame 158 (2011) 2338-2357.
[18] P. Dagaut, C. Togbe, Experimental and modeling study of the kinetics of oxidation of ethanol-n-heptane mixtures in a jet-stirred reactor, Fuel 89 (2010) 280-286.
[19] N. Belhadj, R. Benoit, P. Dagaut, M. Lailliau, Experimental characterization of n-heptane low-temperature oxidation products including keto-hydroperoxides and highly oxygenated organic molecules (HOMs), Combust. Flame 224 (2021) 83-93.
[20] S.S. Wang, R.H. Kong, X.B. Shan, Y.W. Zhang, L.S. Sheng, Z.Y. Wang, L.Q. Hao, S.K. Zhou, Performance of the atomic and molecular physics beamline at the National Synchrotron Radiation Laboratory, J. Synchrotron. Radiat. 13 (2006) 415-420.
[21] Q. Xu, B. Liu, W. Chen, T. Yu, Z. Zhang, C. Zhang, L. Wei, Z. Wang, Comprehensive study of the low-temperature oxidation chemistry by synchrotron photoionization mass spectrometry and gas chromatography, Combust. Flame 236 (2022) 111797.
[22] P. Dagaut, M. Cathonnet, J.P. Rouan, R. Foulatier, A. Quilgars, J.C. Boettner, F. Gaillard, H. James, A jet-stirred reactor for kinetic studies of homogeneous gas-phase reactions at pressures up to ten atmospheres (≈1 MPa), J. Phys. E: Sci. Instrum. 19 (1986) 207-209.
[23] P. Dagaut, M. Cathonnet, J.C. Boettner, F. Gaillard, Kinetic Modeling of Ethylene Oxidation, Combust. Flame 71 (1988) 295-312.
[24] P. Dagaut, C. Togbe, Experimental and modeling study of the kinetics of oxidation of ethanol-gasoline surrogate mixtures (E85 surrogate) in a jet-stirred reactor, Energy Fuels 22 (2008) 3499-3505.
[25] C. Togbe, F. Halter, F. Foucher, C. Mounaim-Rousselle, P. Dagaut, Experimental and detailed kinetic modeling study of 1-pentanol oxidation in a JSR and combustion in a bomb, Proc. Combust. Inst. 33 (2011) 367-374.
[26] Z. Serinyel, C. Togbe, A. Zaras, G. Dayma, P. Dagaut, Kinetics of oxidation of cyclohexanone in a jet-stirred reactor: Experimental and modeling, Proc. Combust. Inst. 35 (2015) 507-514.
[27] T. Javed, E.F. Nasir, A. Ahmed, J. Badra, K. Djebbi, M. Beshir, W.Q. Ji, S.M. Sarathy, A. Farooq, Ignition delay measurements of light naphtha: A fully blended low octane fuel, Proc. Combust. Inst. 36 (2017) 315-322.
[28] E.R. Ritter, J.W. Bozzelli, THERM: Thermodynamic property estimation for gas phase radicals and molecules, Int. J. Chem. Kinet. 23 (1991) 767-778.
[29] S. Xu, R.S. Zhu, M.C. Lin, Ab initio study of the OH + CH_2O reaction: The effect of the OH··OCH2 complex on the H-abstraction kinetics, Int. J. Chem. Kinet. 38 (2006) 322-326.
[30] L.L. Xing, J.W.L. Bao, Z.D. Wang, F. Zhang, D.G. Truhlar, Degradation of Carbonyl Hydroperoxides in the Atmosphere and in Combustion, J. Am. Chem. Soc. 139 (2017) 15821-15835.
[31] Z.D. Wang, O. Herbinet, N. Hansen, F. Battin-Leclerc, Exploring hydroperoxides in combustion: History, recent advances and perspectives, Prog. Energy Combust. Sci. 73 (2019) 132-181.
[32] S.M. Villano, L.K. Huynh, H.H. Carstensen, A.M. Dean, High-Pressure Rate Rules for Alkyl + O_2 Reactions. 2. The Isomerization, Cyclic Ether Formation, and beta-Scission Reactions of Hydroperoxy Alkyl Radicals, J. Phys. Chem. A 116 (2012) 5068-5089.
[33] S.M. Villano, L.K. Huynh, H.H. Carstensen, A.M. Dean, High-Pressure Rate Rules for Alkyl + O_2 Reactions. 1. The Dissociation, Concerted Elimination, and Isomerization Channels of the Alkyl Peroxy Radical, J. Phys. Chem. A 115 (2011) 13425-13442.

[34] A. Miyoshi, Systematic Computational Study on the Unimolecular Reactions of Alkylperoxy (RO_2), Hydroperoxyalkyl (QOOH), and Hydroperoxyalkylperoxy (O_2QOOH) Radicals, J. Phys. Chem. A 115 (2011) 3301-3325.
[35] C.F. Goldsmith, S.J. Klippenstein, W.H. Green, Theoretical rate coefficients for allyl + HO_2 and allyloxy decomposition, Proc. Combust. Inst. 33 (2011) 273-282.
[36] Y. Fenard, H. Song, H. Minwegen, P. Parab, C.S. Mergulhao, G. Vanhove, K.A. Heufer, 2,5-Dimethyltetrahydrofuran combustion: Ignition delay times at high and low temperatures, speciation measurements and detailed kinetic modeling, Combust. Flame 203 (2019) 341-351.
[37] K.W. Zhang, C. Banyon, C. Togbe, P. Dagaut, J. Bugler, H.J. Curran, An experimental and kinetic modeling study of n-hexane oxidation, Combust. Flame 162 (2015) 4194-4207.
[38] S. Sharma, S. Raman, W.H. Green, Intramolecular Hydrogen Migration in Alkylperoxy and Hydroperoxyalkylperoxy Radicals: Accurate Treatment of Hindered Rotors, J. Phys. Chem. A 114 (2010) 5689-5701.
[39] C.F. Goldsmith, W.H. Green, S.J. Klippenstein, Role of O_2 + QOOH in Low-Temperature Ignition of Propane. 1. Temperature and Pressure Dependent Rate Coefficients, J. Phys. Chem. A 116 (2012) 3325-3346.
[40] M. Pelucchi, M. Bissoli, C. Cavallotti, A. Cuoci, T. Faravelli, A. Frassoldati, E. Ranzi, A. Stagni, Improved Kinetic Model of the Low-Temperature Oxidation of n-Heptane, Energy Fuels 28 (2014) 7178-7193.
[41] K.A. Sahetchian, R. Rigny, S. Circan, Identification of the Hydroperoxide Formed by Isomerization-Reactions during the Oxidation of Normal-Heptane in a Reactor and CFR Engine, Combust. Flame 85 (1991) 511-514.
[42] K.A. Sahetchian, A. Heiss, R. Rigny, R.I. Benaim, Determination of the Gas-Phase Decomposition Rate Constants of Heptyl-1 and Heptyl-2 Hydroperoxides $C_7H_{15}OOH$, Int. J. Chem. Kinet. 14 (1982) 1325-1337.
[43] F. Battin-Leclerc, O. Herbinet, P.A. Glaude, R. Fournet, Z.Y. Zhou, L.L. Deng, H.J. Guo, M.F. Xie, F. Qi, Experimental Confirmation of the Low-Temperature Oxidation Scheme of Alkanes, Angew. Chem. Int. Edit. 49 (2010) 3169-3172.
[44] Z. Wang, N. Hansen, A.W. Jasper, B. Chen, D.M. Popolan-Vaida, K.K. Yalamanchi, A. Najjar, P. Dagaut, S.M. Sarathy, Cool flame chemistry of diesel surrogate compounds: n-Decane, 2-methylnonane, 2,7-dimethyloctane, and n-butylcyclohexane, Combust. Flame 219 (2020) 384-392.
[45] N. Belhadj, R. Benoit, P. Dagaut, M. Lailliau, B. Moreau, F. Foucher, Low-temperature oxidation of a gasoline surrogate: Experimental investigation in JSR and RCM using high-resolution mass spectrometry, Combust. Flame 228 (2021) 128-141.
[46] N. Belhadj, M. Lailliau, R. Benoit, P. Dagaut, Experimental and kinetic modeling study of n-hexane oxidation. Detection of complex low-temperature products using high-resolution mass spectrometry, Combust. Flame 233 (2021).
[47] L. Ruwe, L. Cai, J. Wullenkord, S.C. Schmitt, D. Felsmann, M. Baroncelli, B. Chen, K. Moshammer, N. Hansen, H. Pitsch, K. Kohse-Höinghaus, Low- and high-temperature study of n-heptane combustion chemistry, Proc. Combust. Inst. 38 (2021) 405-413.
[48] A. Jalan, I.M. Alecu, R. Meana-Paneda, J. Aguilera-Iparraguirre, K.R. Yang, S.S. Merchant, D.G. Truhlar, W.H. Green, New Pathways for Formation of Acids and Carbonyl Products in Low-

Temperature Oxidation: The Korcek Decomposition of gamma-Ketohydroperoxides, J. Am. Chem. Soc. 135 (2013) 11100-11114.
[49] J. Pfaendtner, L.J. Broadbelt, Mechanistic modeling of lubricant degradation. 1. Structure-reactivity relationships for free-radical oxidation, Ind. Eng. Chem. Res. 47 (2008) 2886-2896.
[50] R.K. Jensen, S. Korcek, L.R. Mahoney, M. Zinbo, Liquid-Phase Autoxidation of Organic-Compounds at Elevated-Temperatures .1. Stirred Flow Reactor Technique and Analysis of Primary Products from Normal-Hexadecane Autoxidation at 120-180℃, J. Am. Chem. Soc. 101 (1979) 7574-7584.
[51] R.K. Jensen, S. Korcek, L.R. Mahoney, M. Zinbo, Liquid-Phase Autoxidation of Organic-Compounds at Elevated-Temperatures .2. Kinetics and Mechanisms of the Formation of Cleavage Products in Normal-Hexadecane Autoxidation, J. Am. Chem. Soc. 103 (1981) 1742-1749.
[52] R.K. Jensen, S. Korcek, M. Zinbo, Liquid-Phase Autoxidation of Organic-Compounds at Elevated-Temperatures - Absolute Rate-Constant for Intermolecular Hydrogen Abstraction in Hexadecane Autoxidation at 120-190℃, Int. J. Chem. Kinet. 26 (1994) 673-680.
[53] P.H. Taylor, M.S. Rahman, M. Arif, B. Dellinger, P. Marshall, Kinetic and mechanistic studies of the reaction of hydroxyl radicals with acetaldehyde over an extended temperature range, Symp. (Int.) Combust. 26 (1996) 497-504.
[54] P.H. Taylor, T. Yamada, P. Marshall, The reaction of OH with acetaldehyde and deuterated acetaldehyde: Further insight into the reaction mechanism at both low and elevated temperatures, Int. J. Chem. Kinet. 38 (2006) 489-495.
[55] J. Bugler, K.P. Somers, E.J. Silke, H.J. Curran, Revisiting the Kinetics and Thermodynamics of the Low-Temperature Oxidation Pathways of Alkanes: A Case Study of the Three Pentane Isomers, J. Phys. Chem. A 119 (2015) 7510-7527.